

**Morphology optimization and assessment of the performance limits of high-porosity nanostructured polymer monolithic capillary columns for proteomics analysis**

Dores-Sousa, José Luís; Terryn, Herman; Eeltink, Sebastiaan

*Published in:*  
Analytica Chimica Acta

*DOI:*  
[10.1016/j.aca.2020.05.019](https://doi.org/10.1016/j.aca.2020.05.019)

*Publication date:*  
2020

*License:*  
CC BY-NC-ND

*Document Version:*  
Accepted author manuscript

[Link to publication](#)

*Citation for published version (APA):*  
Dores-Sousa, J. L., Terryn, H., & Eeltink, S. (2020). Morphology optimization and assessment of the performance limits of high-porosity nanostructured polymer monolithic capillary columns for proteomics analysis. *Analytica Chimica Acta*, 1124, 176-183. <https://doi.org/10.1016/j.aca.2020.05.019>

**Copyright**

No part of this publication may be reproduced or transmitted in any form, without the prior written permission of the author(s) or other rights holders to whom publication rights have been transferred, unless permitted by a license attached to the publication (a Creative Commons license or other), or unless exceptions to copyright law apply.

**Take down policy**

If you believe that this document infringes your copyright or other rights, please contact [openaccess@vub.be](mailto:openaccess@vub.be), with details of the nature of the infringement. We will investigate the claim and if justified, we will take the appropriate steps.

**Morphology optimization and assessment of the performance limits of high-porosity nanostructured polymer monolithic capillary columns for proteomics analysis**

José Luís Does-Sousa<sup>1</sup>, Herman Terry<sup>2</sup>, and Sebastiaan Eeltink<sup>1\*</sup>

<sup>1</sup>Vrije Universiteit Brussel (VUB), Department of Chemical Engineering, Brussels, Belgium

<sup>2</sup>Vrije Universiteit Brussel (VUB), Department of Materials and Chemistry, Brussels, Belgium

(\*) corresponding author

Pleinlaan 2, B-1050, Brussels, Belgium

Tel.: +32 (0)2 629 3324, Fax: +32 (0)2 629 3248, E-mail: [seeltink@vub.be](mailto:seeltink@vub.be)

## Abstract

This study targets the synthesis of high external-porosity poly(styrene-*co*-divinylbenzene) monolithic support structures with macropore and globule sizes in the sub-micron range, aiming at the realization of high-speed and high-resolution gradient separations of intact proteins and peptides. The thermodynamic and kinetic aspects of the free-radical polymerization synthesis were adjusted by tuning the porogen to monomer ratio, the porogen ratio, the initiator content, and polymerization temperature. Next, column morphology was linked to eddy-dispersion and mobile-phase mass-transfer contributions and the chromatographic performance limits were benchmarked against conventional packed columns and silica monoliths. Polymer monolithic structures yielding a separation impedance as low as 976 were created allowing to generate  $N > 1,000,000$  (for an unretained marker), albeit the expense of very long analysis times. Decreasing the macropore and globule sizes below a certain threshold led to significant increase in eddy dispersion, as globular entities agglomerate, and a small number of large flow-through pores permeate the overall fine interconnected polymer network with small diameter flow-through pores. The potential of monolith chromatography for proteomics application is demonstrated with a ballistic 6 s gradient separation of intact proteins and a high-resolution nanoLC-Orbitrap mass spectrometric analysis of a tryptic *E. coli* digest applying a coupled-column system.

**Keywords:** eddy dispersion; separation impedance; kinetic plot; UHPLC; proteins; peptides column technology.

## 1. Introduction

Rigid methacrylate-based polymer-monolithic stationary phases were introduced in large conduit column formats in 1992 by Svec and Fréchet as an alternative for microparticulate columns, targeting high-speed gradient LC separation of intact proteins [1]. Huber *et al.* demonstrated the potential of poly(styrene-*co*-vinylbenzene) monolithic stationary phases synthesized *in-situ* in capillary formats for high-resolution gradient separations of 30 oligonucleotides under 10 min [2]. Since then, the number of published papers describing novel polymer monolithic materials and their applications for biomolecule analysis in separation science is steadily rising [3-7].

The main advantages of monolith technology over packed columns include the ease of *in-situ* column synthesis starting from liquid precursors [8,9] and the low carry-over characteristics for biomolecules due to the absence of (accessible) mesopores and the nature of the polymer surface chemistry [10]. The efficiency of packed columns is related to particle size, but the external porosity is fixed due to the presence of a sphere packing. Monolithic chromatographic support structures have the potential to perform intrinsically better with respect to kinetic performance. This is due to the fact that external porosity can be to a large extent influenced by the monomer to porogen ratio applied and the macropore and globule sizes can be tuned by adjusting the thermodynamic and kinetic conditions during monolith synthesis. A series of papers describing the key factors defining the morphology have been published by the research group of Svec and Fréchet [11-16], Irgum [17, 18], and Eeltink [10,19-21], among many others, including [22-26]. Still, the current possibilities and limitations of precisely tuning the morphology of polymer-monolithic chromatographic substrates are yet to be fully explored.

Different performance indices have been introduced to describe and quantify the chromatographic performance of columns and separation systems [27,28]. In 1977, Knox and Bristow introduced the separation impedance ( $E$ ) taking into account the plate height,  $H$  and hence considering the eddy dispersion ( $A$ -term), longitudinal diffusion ( $B$ -term), and resistance to mass-transfer ( $C$ -term) contributions to chromatographic dispersion, and the chromatographic permeability ( $K_{v,0}$ ) as [29]:

$$E = \frac{H^2}{K_{v,0}} \quad (1)$$

Minimizing  $E$  involves minimizing  $H$  by operating columns at their optimal linear velocity corresponding to the minimum in the van Deemter curve [27]. Minimizing  $H$  involves also reducing the globule size and diameter of the flow-through pores of monolithic support structures, as these sizes affect the magnitude of  $A$ -term and the  $C_m$ -term contributions. Note that convection mainly transports analytes in parallel with the stationary phase surface [19], but the transport towards the stationary-phase surface is driven by diffusion and its magnitude on  $H$  is dependent on the square of the macropore diameter. Minimizing the flow-through pore diameter negatively affects  $K_{v,0}$ . Hence, to increase  $K_{v,0}$  meanwhile reducing the flow-through pore diameter, the number of permeating flow-through pores needs to be maximized [19,30]. A key aspect here is that the structure homogeneity is maintained [30].

Targeting high-resolution biomolecule separations in gradient mode, the aim of this study was to explore the possibilities and limitations of synthesizing high external-porosity polymer monolithic structures with polymer globules and flow-through pores in the submicron range. Therefore, the thermodynamic and kinetic conditions during polymer synthesis were systematically varied and the resulting morphologies were visualized by field-

emission scanning electron microscopy to assess column homogeneity. Selected monolithic columns were subjected to subsequent comprehensive characterization in isocratic LC mode allowing to link column structure to kinetic performance limits. The optimized monolithic support structure was used in gradient mode and the potential for high-speed and high-resolution gradient separations of intact proteins and peptides is demonstrated.

## **2. Materials and methods**

### *2.1. Chemicals and materials*

2,2'-azobis(2-methylpropionitrile) (AIBN, 98%), 1-decanol ( $\geq 98\%$ ), divinylbenzene (DVB, 80%), styrene (S,  $\geq 99\%$ ), tetrahydrofuran (THF, anhydrous, inhibitor-free,  $\geq 99.9\%$ ), toluene (anhydrous, 99.8%), 3-(trimethoxysilyl)propyl methacrylate (98%),  $\alpha$ -chymotrypsin A from bovine pancreas ( $\geq 85\%$ ),  $\alpha$ -chymotrypsinogen from bovine pancreas,  $\alpha$ -lactalbumin from bovine milk ( $\geq 85\%$ ), carbonic anhydrase from bovine erythrocytes ( $\geq 95\%$ ), cytochrome *c* from bovine heart ( $\geq 95\%$ ), cytochrome *c* from equine heart ( $\geq 95\%$ ), insulin from bovine pancreas, lysozyme from chicken egg white ( $\geq 90\%$ ), myoglobin from equine heart ( $\geq 90\%$ ), ribonuclease A from bovine pancreas, and trypsin from bovine pancreas ( $\geq 90\%$ ) were purchased from Sigma-Aldrich (Zwijndrecht, The Netherlands). *E. coli* protein sample (lyophilized) was obtained from Bio-Rad Laboratories (Temse, Belgium). Aluminium oxide (90 active neutral), hydrochloric acid (32%) and sodium hydroxide pellets were purchased from Merck (Darmstadt, Germany). Acetonitrile (ACN, HPLC supra-gradient quality), formic acid (FA, 99%), and trifluoroacetic acid (TFA, 99.0%) were purchased from Biosolve (Valkenswaard, The Netherlands). The SMART Digest trypsin kit was obtained from Thermo Fisher Scientific (Sunnyvale, CA, USA). Deionized water (18.2

M $\Omega$ ·cm) was purified in-house using a Milli-Q water-purification system (Millipore, Molsheim, France). Polyimide-coated fused-silica capillary tubing was purchased from Polymicro Technologies (Molex B.V, Eindhoven, The Netherlands).

## 2.2 Monolith synthesis

Polymer monolithic columns were synthesized *in-situ* in 100  $\mu$ m i.d.  $\times$  375  $\mu$ m o.d. fused-silica capillaries. To enable covalent attachment of the monolith entity to the inner wall surface, fused-silica capillary was subjected to a pretreatment with 3-(trimethoxysilyl)propyl methacrylate, as previously described by Courtois *et al.* [31]. Prior to monolith synthesis, the polymerization inhibitor tertbutylcatechol was removed from S and DVB by passing the monomers over activated basic alumina columns. An array of polymer monolithic columns with different macropore structures was prepared by thermally-initiated free-radical polymerization for 24 h [12,18,32]. Polymerization mixtures composed of S and DVB (monomers), 1-decanol and THF (porogen), and AIBN (initiator) were prepared with different weight ratios, *i.e.*, S-to-DVB ratios ranging between 50:50% and 20:80% (w/w), 1-decanol:THF ratios ranging between 65:35% and 76:24% (w/w), and 2-4% (w/w) AIBN with respect to total monomer content. Next, polymerization precursor mixtures were stirred and degassed in an ultrasonic bath for 10 min, respectively. Capillaries were filled with the respective mixtures by means of a syringe and in- and outlets were sealed with silicone caps. The polymerization reaction was carried out in a water bath (Julabo, Seelbach, Germany) for 24 h. Polymerization temperatures were varied between 65 to 75°C in steps of 5°C. Afterwards, the monolithic columns were immediately flushed at a flow rate of 300 nL·min<sup>-1</sup> for 2 h with 80:20% (v/v) ACN:H<sub>2</sub>O.

### 2.3. Instrumentation and conditions

Field-emission scanning electron microscopy (SEM) images of cross-section surfaces of monolithic capillary columns were obtained with a JSM-6400 field-emission scanning electron microscope (JEOL, Tokyo, Japan) after sputtering a 6 nm thick Pt-Pd coating applying a 208 HR sputter coater equipped with a Cressington MTM-20 thickness controller (Cressington Scientific Instruments, Watford, UK). Images with magnifications up to 35.000x were captured applying acceleration voltages of 5 kV.

Chromatographic experiments were performed using an Ultimate 3000 RSLCnano system (Thermo Fisher Scientific, Germering, Germany) equipped with a NCS-3500RS binary high-pressure gradient pump, a 4 nL injection valve (Valco, Schenkon, Switzerland), and a VWD-3400RS UV detector equipped with a 3-nL  $z$ -shaped flow cell ( $\lambda = 254$  nm, 20-100 Hz data collection rate and 0.12-0.03 s response time). Chromeleon software (version 6.8, Rev. SR14, Thermo Fisher Scientific) was used for instrument control and data management. Plate numbers in isocratic mode were determined by injection of uracil. Protein separations were executed applying linear aqueous-ACN gradients from 20 to 48% (v/v) ACN with 0.05% (v/v) TFA added to the mobile-phase as ion-pairing agent. LC-MS profiling experiments were performed on a RSLCnano system coupled to an Orbitrap LTQ XL mass spectrometer (Thermo Fisher Scientific, Bremen, Germany) via a nanoESI interface. For the digestion of *E. coli* protein sample, 150  $\mu$ L of SMART Digest buffer solution were added to 50  $\mu$ L of sample with a concentration of 0.675 mg·mL<sup>-1</sup>, according to manufacturer instructions. The sample was incubated at 70 °C for 5 h, and then cleaned up by centrifugation at 5,000 rpm for 15 min. For this experiment, 0.1% (v/v) FA was added as ion-pairing agent

to the mobile phase. The MS was operated in positive ionization mode, and the nanoESI parameters were as follows: spray voltage: 2.30 kV; capillary voltage: 30 V; capillary temperature: 200°C; tube lens: 195 V. Experiments covering masses in the  $m/z$  300-2000 range and at the resolution of 30,000 were carried out. The data acquisition software used was Xcalibur (version 2.1.0, Thermo Fisher Scientific).

### **3. Results and discussion**

#### *3.1. Tuning of the macropore structure*

Key variables in the optimization of the porous monolithic substrates are the amount of monomer together with the porogen ratio in the polymerization mixture. The porogen to monomer ratio was varied at four different levels, *i.e.*, 80:20, 75:25, 70:30, and 60:40% (w/w). We found that fixing the porogen to monomer ratio at 75:25% (w/w) led to monolithic substrates with higher permeability, while having good structural integrity providing the desired mechanical stability for high-pressure operation. THF and 1-decanol were selected as porogenic solvents, in which THF, characterized by a large electronegativity induced by the oxygen atom, acts a thermodynamic ‘good’ solvent with respect to the polymer, while 1-decanol acts as a ‘poor’ solvent. Varying the porogen ratio allowed for tuning of the globule and macropore size over more than one order of magnitude. Fig. 1 shows field-emission scanning electron micrographs (SEM’s) of fracture cross-section surfaces of monolithic capillary columns at two different magnification levels. Increasing the THF to 1-decanol ratio generally led to a decrease in microglobule and macropore diameters. Applying over 22 wt% of THF in the polymerization mixture, it can be observed that polymer globular entities start to agglomerate leading to larger clusters, while a small number of large diameter flow-

through pores perfuse the polymer substrate in parallel to a network of small diameter macropores. The average microglobule size was estimated from SEM images for selected columns and the determination of frequency distributions from over 50 measurements, see Fig. S1 in the Supplementary Material. The mechanical stability up to 400 bar column pressure is demonstrated in Fig. S2

Fig. 2 visualizes the contribution of the reaction kinetics, *i.e.*, polymerization temperature and initiator concentration, on the resulting macropore structures while maintaining the porogen to monomer ratio and porogen ratio constant. At elevated temperature the rate of initiation, the number of growing radicals, and the polymerization rate will be higher. As a result, more nuclei are formed which means their size will remain relatively small. When the polymerization temperature is lowered, the polymerization rate is slow, and the remaining monomers can be transferred from the solution to the nuclei. This negatively translates into the formation of larger pores and hence lowers the available surface area.

### *3.2. Assessment of dispersion characteristics*

Assessment of chromatographic performance included benchmarking columns in isocratic mode to establish experimental van Deemter curves [20] and conducting flow-pressure experiments to determine column permeabilities ( $K_v$ ), based on the Darcy equation [33,34]. Fig. 3 shows the eddy dispersion (A-term) and mobile-phase mass transfer ( $C_m$ -term) contributions estimated by applying a non-linear fit of the van Deemter curve as function of the average microglobule size (experimental van Deemter curves are displayed in Fig. S3). Decreasing the macropore and globule size induced by increasing the THF content in the

polymerization mixtures led to a reduction in both the  $A$ - and  $C_m$ -term, due to the smaller globule size and flow-through pore diameter. The decrease in the  $C$ -term contribution is more pronounced, which may be expected as the magnitude of the  $A$ -term is proportional to domain size and  $C_m$  is proportional to square of the macropore diameter.

The best performing monolithic column yielded a minimum plate height of 8.7  $\mu\text{m}$  at optimum mobile-phase velocity ( $\sim 115.000$  plates/meter), with  $A = 3.6 \mu\text{m}$  and  $C_m = 5.2 \text{ ms}$ , see Fig. 1C-D for the corresponding morphology. Increasing the THF content above 21 wt% resulted in a strong increase in both the  $A$ - and  $C$ -term contributions. This effect can be explained by the presence of (a small number of) larger macropores and also some polymer agglomerate clusters. Furthermore, the increase in polydispersity in morphology of the smaller-domain-size monoliths led to a significantly rise in  $A$ -term.

To assess and compare the intrinsic quality of chromatographic support structures, the column permeability, which is a one of the key drivers for stationary-phase development together with efficiency and selectivity, should be considered in addition to dispersion effects. The kinetic performance of a system can be visualized in a geometry-independent manner, in which column-length/domain-size combinations are exploited to generate the highest separation efficiency within the shortest analysis time, while operating the system at a  $\Delta P_{\text{max}}$ . Fig. 4A shows the kinetic performance limits of polymer monolithic columns with different porous structures, applying Eq. 2 and 3 and operating at a maximum column pressure ( $\Delta P_{\text{max}}$ ) of 400 bar [28].

$$N = \frac{\Delta P_{\text{max}}}{\eta} \cdot \left( \frac{K_v}{u_0 \cdot H} \right)_{\text{exp}} \quad (2)$$

$$t_0 = \frac{\Delta P_{max}}{\eta} \cdot \left( \frac{K_v}{u_0^2} \right)_{exp} \quad (3)$$

where  $N$  is the number of plates when operating columns at the kinetic performance limit,  $\eta$  the mobile-phase viscosity,  $u_0$  the linear mobile-phase velocity, and  $H$  the plate height. The monolith featuring large globule and macropores size, characterized by high permeability ( $K_v = 2.6 \times 10^{-12} \text{ m}^2$ ), allows to generate over 1,000,000 plates when using long columns, but at the expense of long analysis times. To advance the speed of analysis, monoliths with smaller macropore and globule size (limiting diffusion distances and eddy dispersion) were developed. This led to the development of porous monolithic support structures with  $K_v = 7.8 \times 10^{-14} \text{ m}^2$  (21 wt% THF in the porogen), yielding the best compromise in terms of peak-production rate for  $N < 1,000,000$ . This represents approximately up to 20 times higher permeability values than a column packed with  $1.5 \text{ }\mu\text{m}$  core-shell particles [35], and up to 2-4 for the 1<sup>st</sup> and 2<sup>nd</sup> generation of silica monoliths [36, 37], respectively. Further downscaling the feature size resulted in an increase in  $A$ - and  $C$ -term contribution concomitant with a decrease in  $K_v$ . This contributed to a significant loss in performance characterized by subsequent shift of kinetic performance curves to the left.

Fig. 4B shows the comparison of the chromatographic performance of selected support structures, *i.e.*, the polymer monolith yielding the best peak-production rate for  $N < 1,000,000$ , columns packed with  $2.6 \text{ }\mu\text{m}$  and  $1.5 \text{ }\mu\text{m}$  core-shell particles with data obtained from literature [35], and first- and second-generation silica monoliths [37]. Note that the separation impedance is plotted as function of the number of plates that can be generated operating columns at a 400 bar in an inverted x-axis. In this representation, the trend for each individual curve follows a van Deemter type curve, having the  $B$ -term dominated region on

the left, and the  $C$ -term dominated region at the righthand side. The separation impedance of the polymer monoliths ( $E = 976$ ) was significantly lower than that of packed columns and silica monolithic structures. The 2.6 and 1.5  $\mu\text{m}$  particle-packed columns exhibit a minimum  $E$  value of  $\sim 1500$ -3000, but 1.5  $\mu\text{m}$  particle-packed columns perform better for fast separation due to the minimized  $C$ -term contribution, and the curve shifts horizontally to the left when applying large particle diameter (in case of self-similar structure as it is the case for packed columns) as longer columns can be employed. The polymer monoliths can outperform the particulate columns for required plate numbers ( $N_{\text{req}} > 200,000$ ), however this high resolving power is only obtained at very long (unpractical) analysis times. As such, in isocratic operation mode, the current polymer-monoliths support structure cannot compete with conventional particle-packed column technology in terms of plate number per unit time. This can be mainly attributed to the increase in structural inhomogeneity when downscaling dimensions. Table S1 (see in the Supplementary Material) summarizes the chromatographic properties of the synthesized monolithic columns, focusing on the influence of the kinetic and thermodynamic properties of the reaction on the dispersion characteristics. It should be noted that even smaller  $E$  values were attained ( $E = 297$ ), but these columns were characterized by having high permeability values rather than having good structure homogeneity.

### *3.3. Biomolecule profiling in gradient LC mode*

In gradient mode, peak capacity, defined as the maximum number of peaks separated with unit resolution covering the gradient window applied, is the most used performance metric and defined by Neue as [38, 39]:

$$n_c = 1 + \frac{\sqrt{N}}{4} \cdot \frac{S \cdot \Delta c}{S \cdot \Delta c \cdot \frac{t_0}{t_G} + 1} \quad (4)$$

where  $S$  is defined as the slope of the linear dependency of  $\ln k$  versus the volume fraction of organic solvent in the mobile phase and  $\Delta c$  is the gradient span. The maximum number of plates (in isocratic mode) is achieved when operating a column at  $\Delta P_{max}$  and the length should be adjusted such that the flow rate corresponds to  $u_{opt}$ . In order to reach the maximum peak capacity per unit time in gradient mode, *i.e.*, to work at the kinetic performance limits, the flow rate and column length should be adjusted such that columns are operated at the maximum system pressure. At the same time, the flow rate should be a factor 2-4 higher than the  $u_{opt}$  to fully benefit from the effect of the gradient volume on  $n_c$  [38,40,41]. For clarity, Fig 4B depicts performance limit data when operating in isocratic mode. The highlighted colored boxes in the figure depict the optimal flow rate (shifted into the C-term region) when operating in gradient mode and where peak capacity is maximized. Now it becomes apparent that in gradient mode polymer monoliths provide unique separation potential compared to conventional columns targeting high-resolution separations with long columns, *e.g.*, for profiling of complex life-science biomolecule mixtures. Table 1 provides an overview of peak capacities that can be generated in gradient mode when conducting column-coupling experiments, while operating at kinetic performance limits (see the Supplementary Materials for a more detailed explanation). Furthermore, Table 1 displays good column-to-column repeatability.

Fig. 5A shows an example of high resolving power (average peak capacity of 91) provided by monolith chromatography for the separation of 10 intact proteins, which was achieved in an analysis time of only 3.5 min. TFA was selected as ion pairing agent as this

ion pairing provided better mass loadability (narrower peaks) compared to FA. When working at the kinetic performance limits ( $\Delta P_{max} = 400$  bar) the potential of a 70 mm short polymer monolithic capillary column was demonstrated for ultra-fast protein separations and applying a ballistic gradient of only 6 seconds, see Fig. 5B. For this separation, extra-column dispersion and time contributions were minimized by mounting the column directly on the stator of a 4 nL valve and using 20  $\mu\text{m}$  i.d.  $\times$  100 mm connection tubing towards a 3 nL flow cell. The separation of 6 proteins was achieved within a cycle time of only 12 s, which includes a 3 s wash step and column equilibration. The high resolving power of monolith chromatography (column length of 920 mm yielding 106,000 plates in isocratic mode (for an unretained marker), optimized pore structure, and applying a gradient time of 240 min at the kinetic performance limit with  $\Delta P_{max} = 400$  bar) for the separation of a proteolytic digest of *E. coli* proteins is shown in Fig. 6. The latter experiment was achieved by coupling four capillary columns using zero-dead-volume unions and using FA as ion pairing agent providing greater ionization and detection sensitivity.

#### **4. Concluding remarks**

High-porosity monolithic stationary phases with different macropore structures have been synthesized and dispersion contributions and column permeabilities have been assessed. Monolithic support structures yielding minimum plate-height values as low as 8.7  $\mu\text{m}$  and separation impedance values as low as 976 have been developed. The latter value is mainly defined by the high column permeabilities obtained. In isocratic mode, the monolithic support structures have the potential to outperform conventional column technologies for  $N > 200,000$  (based on measurements using an unretained marker), when applying very long

columns, which results into unpractically long analysis times. Note that also the use of conventional (S-*co*-DVB) polymer monolithic materials for small molecule analysis are generally limited due to significant stationary phase mass-transfer contributions to peak broadening [42-45]. Downscaling characteristic feature sizes (flow-through pore and globule size) was not feasible, as structure inhomogeneity negatively affects dispersion characteristics. However, when operating columns above the optimum van Deemter flow rate to maximize peak capacity in gradient mode, monolith chromatography has the ability to outperform conventional columns when targeting high-resolution proteomics profiling applications. We have also demonstrated the potential of monolith chromatography for high-throughput analysis, with cycle times down to 12 s. This may open new approaches for the application of these high-porosity structures in two-dimensional liquid chromatography as second dimension columns.

Having excellent control over structure homogeneity is critical to further advance monolith technology and surpass the current performance boundaries. By using traditional polymerization approaches, it is unlikely that the macropore and globule size distributions can be controlled such that the size distributions scale down with domain size. Alternatively, novel synthesis approaches than can be explored include the use of structure-directing agents, such as ice crystals, or self-assembly of nanostructures, which can be removed after the polymerization reaction leaving templated macropores. Also, 3D printing technology is rapidly advancing. Direct writing approaches to target *in-situ* micro and nanostructures on a polymer resin are already at hand. For example, three-dimensional nanostructures have been created using two-photon polymerization [46]. However, major limitations include the high cost and the relatively slow writing speed.

## 5. Acknowledgements

Grants of the Research Foundation Flanders (FWO – grant no. G025916N and G033018N) are gratefully acknowledged. SE acknowledge the Excellence of Science grant (30897864) of the FWO-FNRS. The authors thank Dr. Rob van der Hoeven (DSM Technology Center, The Netherlands) and Franck van Veen (Thermo Fisher Scientific, The Netherlands) for their help with the Orbitrap mass spectrometer.

## 6. References

- [1] F. Svec, J.M.J. Frechet, Continuous rods of macroporous polymer as high-performance liquid chromatography separation media, *Anal. Chem.*, 64 (1992) 820-822.
- [2] A. Premstaller, H. Oberacher, C.G. Huber, High-performance liquid chromatography–electrospray ionization mass spectrometry of single- and double-stranded nucleic acids using monolithic capillary columns, *Anal. Chem.*, 72 (2000) 4386-4393.
- [3] J. Urban, Are we approaching a post-monolithic era?, *J. Sep. Sci.*, (2020) 1-6.
- [4] F. Svec, Monolithic columns: A historical overview, *Electrophoresis*, 38 (2017) 2810-2820.
- [5] F. Maya, F. Svec, Porous polymer monoliths with large surface area and functional groups prepared via copolymerization of protected functional monomers and hypercrosslinking, *J. Chromatogr. A*, 1317 (2013) 32-38.
- [6] A. Nordborg, E.F. Hilder, Recent advances in polymer monoliths for ion-exchange chromatography, *Anal. Bioanal. Chem.*, 394 (2009) 71-84.

- [7] R.D. Arrua, M. Talebi, T.J. Causon, E.F. Hilder, Review of recent advances in the preparation of organic polymer monoliths for liquid chromatography of large molecules, *Anal. Chim. Acta*, 738 (2012) 1-12.
- [8] K. Liu, P. Aggarwal, J.S. Lawson, H.D. Tolley, M.L. Lee, Organic monoliths for high-performance reversed-phase liquid chromatography, *J. Sep. Sci.*, 36 (2013) 2767-2781.
- [9] F. Svec, Recent developments in the field of monolithic stationary phases for capillary electrochromatography, *J. Sep. Sci.*, 28 (2005) 729-745.
- [10] S. Eeltink, S. Wouters, J.L. Does-Sousa, F. Svec, Advances in organic polymer-based monolithic column technology for high-resolution liquid chromatography-mass spectrometry profiling of antibodies, intact proteins, oligonucleotides, and peptides, *J. Chromatogr. A*, 1498 (2017) 8-21.
- [11] F. Svec, Quest for organic polymer-based monolithic columns affording enhanced efficiency in high performance liquid chromatography separations of small molecules in isocratic mode, *J. Chromatogr. A*, 1228 (2012) 250-262.
- [12] F. Svec, J.M.J. Fréchet, Temperature, a simple and efficient tool for the control of pore size distribution in macroporous polymers, *Macromolecules*, 28 (1995) 7580-7582.
- [13] F. Svec, J.M.J. Fréchet, Kinetic control of pore formation in macroporous polymers. formation of "molded" porous materials with high flow characteristics for separations or catalysis, *Chem. Mater.*, 7 (1995) 707-715.
- [14] S. Xie, R.W. Allington, J.M.J. Fréchet, F. Svec, Porous polymer monoliths: An alternative to classical beads, in: R. Freitag (Ed.) *Modern Advances in Chromatography*, Springer Berlin Heidelberg, Berlin, Heidelberg, 2002, pp. 87-125.
- [15] E.C. Peters, M. Petro, F. Svec, J.M.J. Fréchet, Molded rigid polymer monoliths as separation media for capillary electrochromatography, *Anal. Chem.*, 69 (1997) 3646-3649.

- [16] E.C. Peters, M. Petro, F. Svec, J.M.J. Fréchet, Molded rigid polymer monoliths as separation media for capillary electrochromatography. 1. Fine control of porous properties and surface chemistry, *Anal. Chem.*, 70 (1998) 2288-2295.
- [17] E. Byström, C. Viklund, K. Irgum, Differences in porous characteristics of styrenic monoliths prepared by controlled thermal polymerization in molds of varying dimensions, *J. Sep. Sci.*, 33 (2010) 191-199.
- [18] C. Viklund, F. Svec, J.M.J. Fréchet, K. Irgum, Monolithic, “molded”, porous materials with high flow characteristics for separations, catalysis, or solid-phase chemistry: control of porous properties during polymerization, *Chem. Mater*, 8 (1996) 744-750.
- [19] J.L. Dores-Sousa, A. Fernández-Pumarega, J. De Vos, M. Lämmerhofer, G. Desmet, S. Eeltink, Guidelines for tuning the macropore structure of monolithic columns for high-performance liquid chromatography, *J. Sep. Sci.*, 42 (2019) 522-533.
- [20] S. Wouters, T. Hauffman, M.C. Mittelmeijer-Hazeleger, G. Rothenberg, G. Desmet, G.V. Baron, S. Eeltink, Comprehensive study of the macropore and mesopore size distributions in polymer monoliths using complementary physical characterization techniques and liquid chromatography, *J. Sep. Sci.*, 39 (2016) 4492-4501.
- [21] S. Wouters, B. Wouters, A. Vaast, H. Terryn, G. Van Assche, S. Eeltink, Monitoring the morphology development of polymer-monolithic stationary phases by thermal analysis, *J. Sep. Sci.*, 37 (2014) 179-186.
- [22] G. Guiochon, Monolithic columns in high-performance liquid chromatography, *J. Chromatogr. A*, 1168 (2007) 101-168.
- [23] N. Tanaka, H. Kobayashi, N. Ishizuka, H. Minakuchi, K. Nakanishi, K. Hosoya, T. Ikegami, Monolithic silica columns for high-efficiency chromatographic separations, *J. Chromatogr. A*, 965 (2002) 35-49.

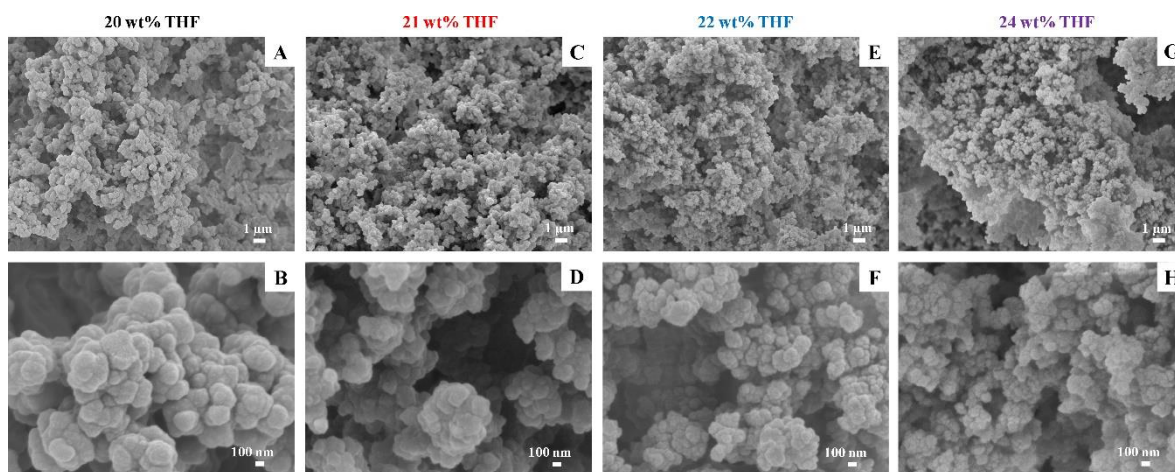
- [24] J. Urban, P. Jandera, Polymethacrylate monolithic columns for capillary liquid chromatography, *J. Sep. Sci.*, 31 (2008) 2521-2540.
- [25] M.R. Buchmeiser, Polymeric monolithic materials: Syntheses, properties, functionalization and applications, *Polymer*, 48 (2007) 2187-2198.
- [26] L. Trojer, C.P. Bisjak, W. Wieder, G.K. Bonn, High capacity organic monoliths for the simultaneous application to biopolymer chromatography and the separation of small molecules, *J. Chromatogr. A*, 1216 (2009) 6303-6309.
- [27] J.L. Dores-Sousa, J. De Vos, S. Eeltink, Resolving power in liquid chromatography: A trade-off between efficiency and analysis time, *J. Sep. Sci.*, 42 (2019) 38-50.
- [28] G. Desmet, D. Clicq, P. Gzil, Geometry-independent plate height representation methods for the direct comparison of the kinetic performance of LC supports with a different size or morphology, *Anal. Chem.*, 77 (2005) 4058-4070.
- [29] P.A. Bristow, J.H. Knox, Standardization of test conditions for high performance liquid chromatography columns, *Chromatographia*, 10 (1977) 279-289.
- [30] J. Billen, G. Desmet, Understanding and design of existing and future chromatographic support formats, *J. Chromatogr. A*, 1168 (2007) 73-99.
- [31] J. Courtois, M. Szumski, E. Byström, A. Iwasiewicz, A. Shchukarev, K. Irgum, A study of surface modification and anchoring techniques used in the preparation of monolithic microcolumns in fused silica capillaries, *J. Sep. Sci.*, 29 (2006) 14-24.
- [32] A. Vaast, H. Terry, F. Svec, S. Eeltink, Nanostructured porous polymer monolithic columns for capillary liquid chromatography of peptides, *J. Chromatogr. A*, 1374 (2014) 171-179.
- [33] C.A. Cramers, J.A. Rijks, C.P.M. Schutjes, Factors determining flow rate in chromatographic columns, *Chromatographia*, 14 (1981) 439-444.

- [34] A.F. Georges Guiochon, Dean G. Shirazi, Fundamentals of preparative and nonlinear chromatography 2nd Edition ed., Elsevier, 2006.
- [35] J. De Vos, M. De Pra, G. Desmet, R. Swart, T. Edge, F. Steiner, S. Eeltink, High-speed isocratic and gradient liquid-chromatography separations at 1500 bar, *J. Chromatogr. A*, 1409 (2015) 138-145.
- [36] D. Cabooter, K. Broeckhoven, R. Sterken, A. Vanmessen, I. Vandendael, K. Nakanishi, S. Deridder, G. Desmet, Detailed characterization of the kinetic performance of first and second generation silica monolithic columns for reversed-phase chromatography separations, *J. Chromatogr. A*, 1325 (2014) 72-82.
- [37] K. Hormann, T. Müllner, S. Bruns, A. Hölzel, U. Tallarek, Morphology and separation efficiency of a new generation of analytical silica monoliths, *J. Chromatogr. A*, 1222 (2012) 46-58.
- [38] M. Gilar, U.D. Neue, Peak capacity in gradient reversed-phase liquid chromatography of biopolymers: Theoretical and practical implications for the separation of oligonucleotides, *J. Chromatogr. A*, 1169 (2007) 139-150.
- [39] U.D. Neue, Peak capacity in unidimensional chromatography, *J. Chromatogr. A*, 1184 (2008) 107-130.
- [40] A. Fernández-Pumarega, J.L. Does-Sousa, S. Eeltink, A comprehensive investigation of the peak capacity for the reversed-phase gradient liquid-chromatographic analysis of intact proteins using a polymer-monolithic capillary column, *J. Chromatogr. A*, 1609 (2020) 460462.
- [41] X. Wang, D.R. Stoll, A.P. Schellinger, P.W. Carr, Peak capacity optimization of peptide separations in reversed-phase gradient elution chromatography: Fixed column format, *Anal. Chem.*, 78 (2006) 3406-3416.

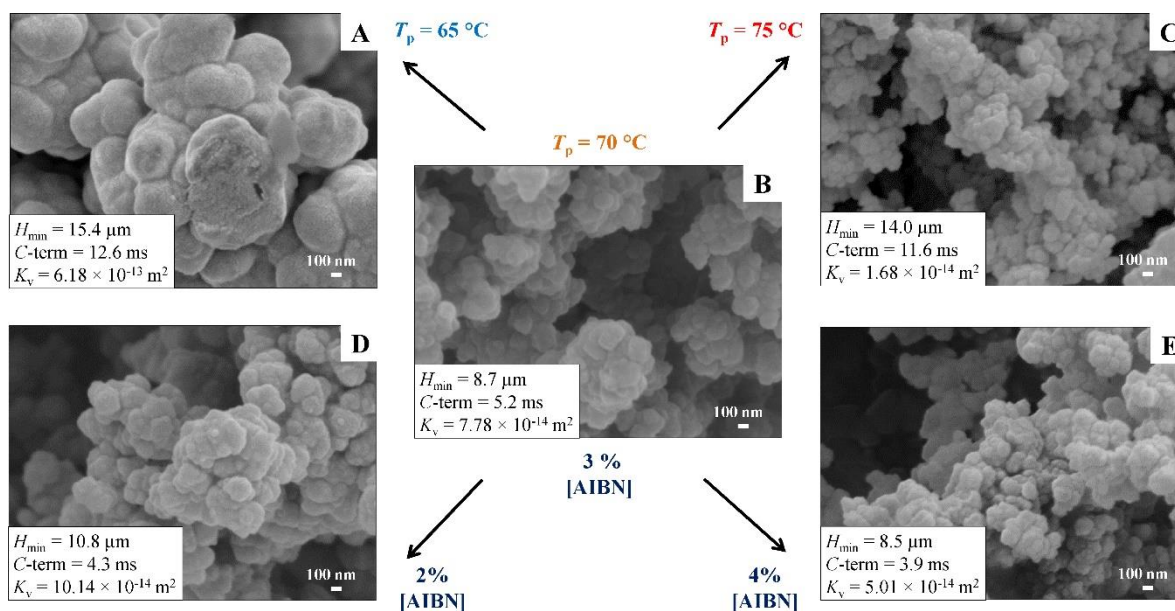
- [42] Y. Huo, P.J. Schoenmakers, W.T. Kok, Efficiency of methacrylate monolithic columns in reversed-phase liquid chromatographic separations, *J. Chromatogr. A*, 1175 (2007) 81-88.
- [43] J. Urban, F. Svec, J.M.J. Fréchet, Hypercrosslinking: New approach to porous polymer monolithic capillary columns with large surface area for the highly efficient separation of small molecules, *J. Chromatogr. A*, 1217 (2010) 8212-8221.
- [44] J. Urban, F. Svec, J.M.J. Fréchet, Efficient separation of small molecules using a large surface area hypercrosslinked monolithic polymer capillary column, *Anal. Chem.*, 82 (2010) 1621-1623.
- [45] T.J. Causon, I. Nischang, Critical differences in chromatographic properties of silica- and polymer-based monoliths, *J. Chromatogr. A*, 1358 (2014) 165-171.
- [46] K. Broeckhoven, D. Cabooter, S. Eeltink, W. De Malsche, F. Matheuse, G. Desmet, Current and future chromatographic columns: is one column enough to rule them all?, *LC GC North Am*, 36 (2018) 9–17.

**Table 1.** Predicted and experimental performances in gradient mode for extrapolated kinetic performance limit conditions ( $\Delta P_{\max} = 400$  bar), applying 1, 2, or 4 coupled columns, and  $t_G/t_0 = 5$ . The experimental peak capacity was obtained by injecting the proteins ribonuclease A, insulin, cytochrome *c* equine, cytochrome *c* bovine, and carbonic anhydrase.

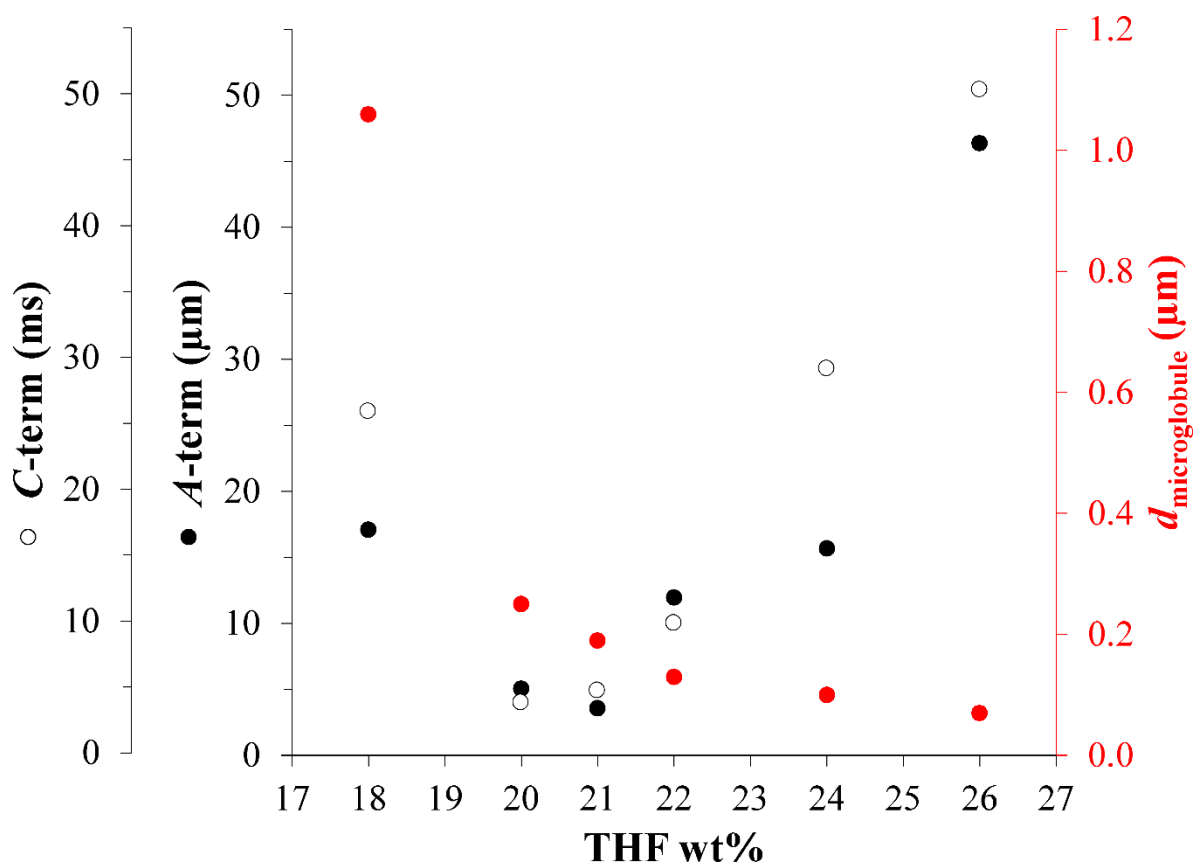
<i>L</i> (mm)	<i>F</i> ( $\mu\text{L}\cdot\text{min}^{-1}$ )	<i>t<sub>g</sub></i> (min)	<i>n<sub>c</sub></i> predicted	<i>n<sub>c</sub></i> experimental	Deviation (%)
70	12	0.2	-	19.4	-
230	3	2.6	71.4	66.7	-7%
230	3	2.6	71.4	67.8	-5%
230	3	2.6	71.4	69.1	-3%
2 × 230	1.5	10.2	105.4	99.5	-6%
4 × 230	0.75	37.2	189.9	149.0	-22%



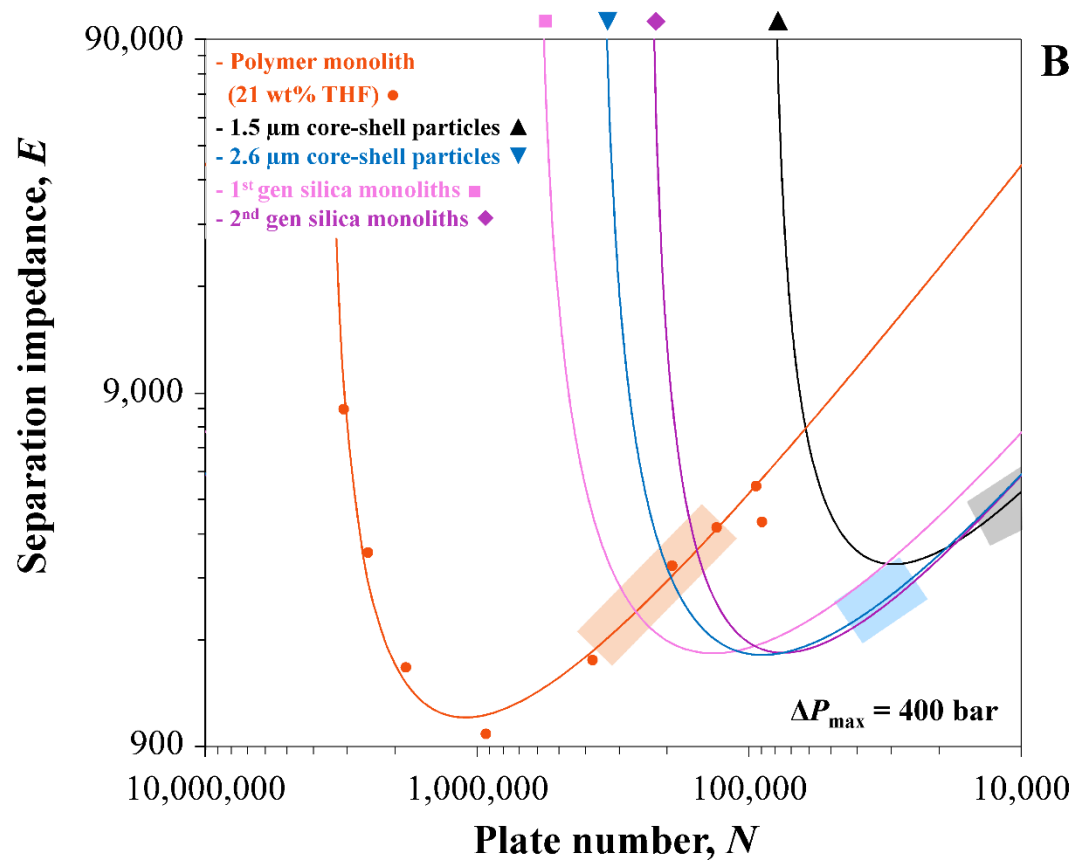
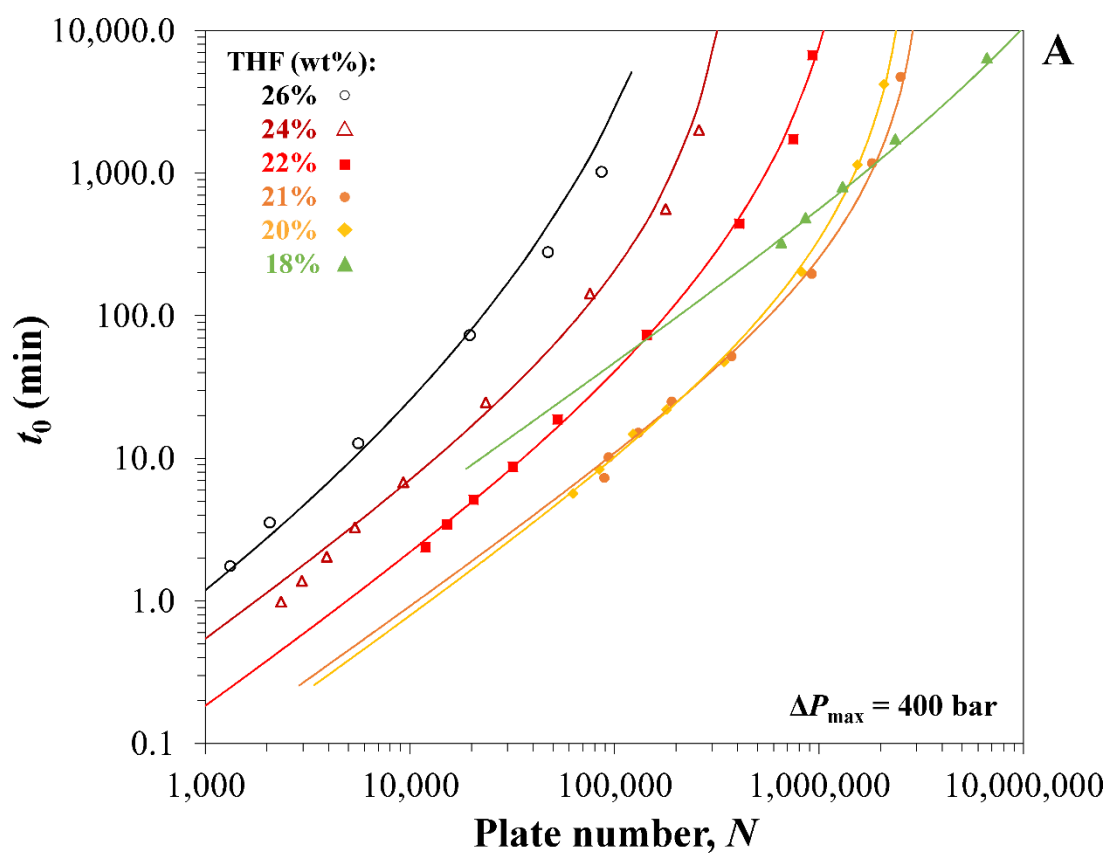
**Figure 1.** Scanning electron micrograph (SEM) images of cross sections of 100  $\mu\text{m}$  i.d. monolithic poly(S-*co*-DVB) capillary columns prepared with a porogen to monomer ratio at 75:25 w/w%, showing the effect of the porogenic solvent ratio content (THF/1-decanol): (A and B) 20 wt% THF, (C and D) 21 wt% THF, (E and F) 22 wt% THF, and (G and H) 24 wt% THF. The bottom micrographs show the respective zoom-ins.



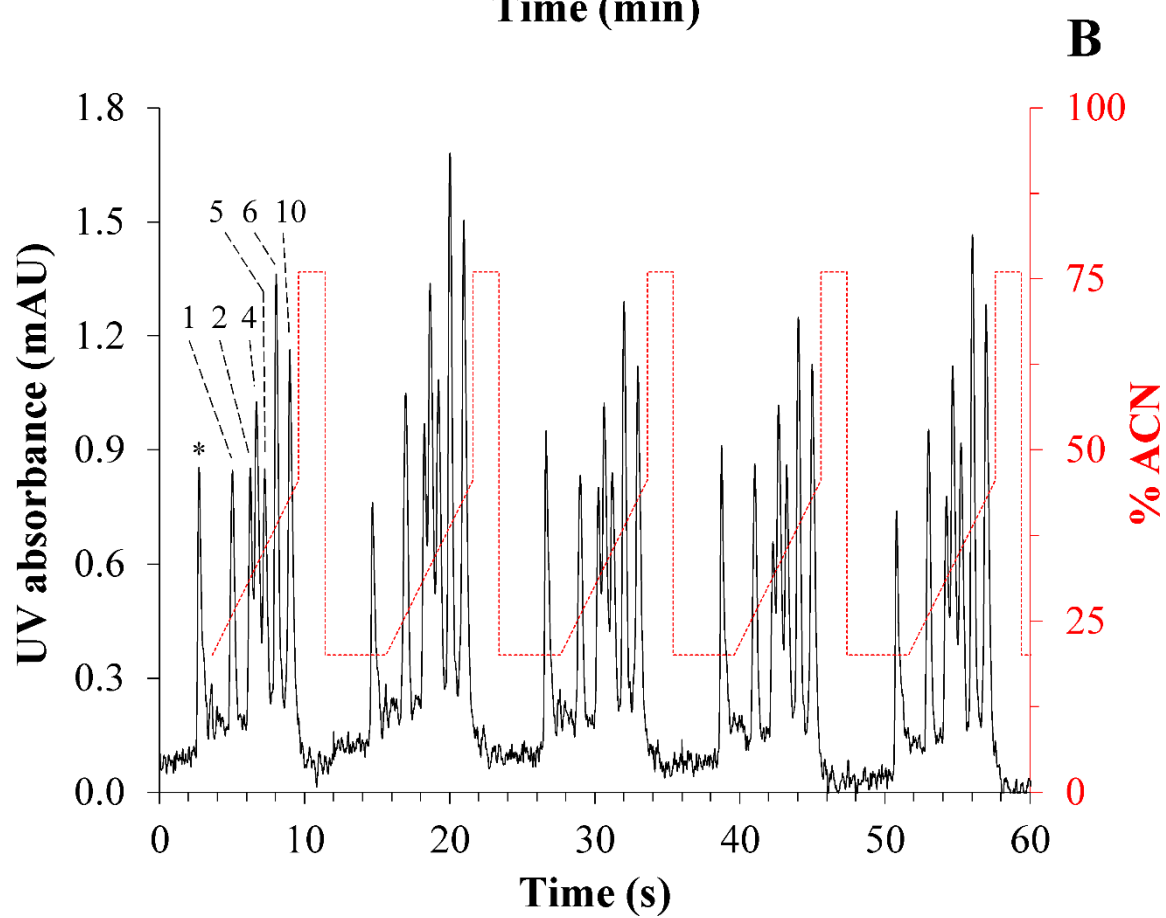
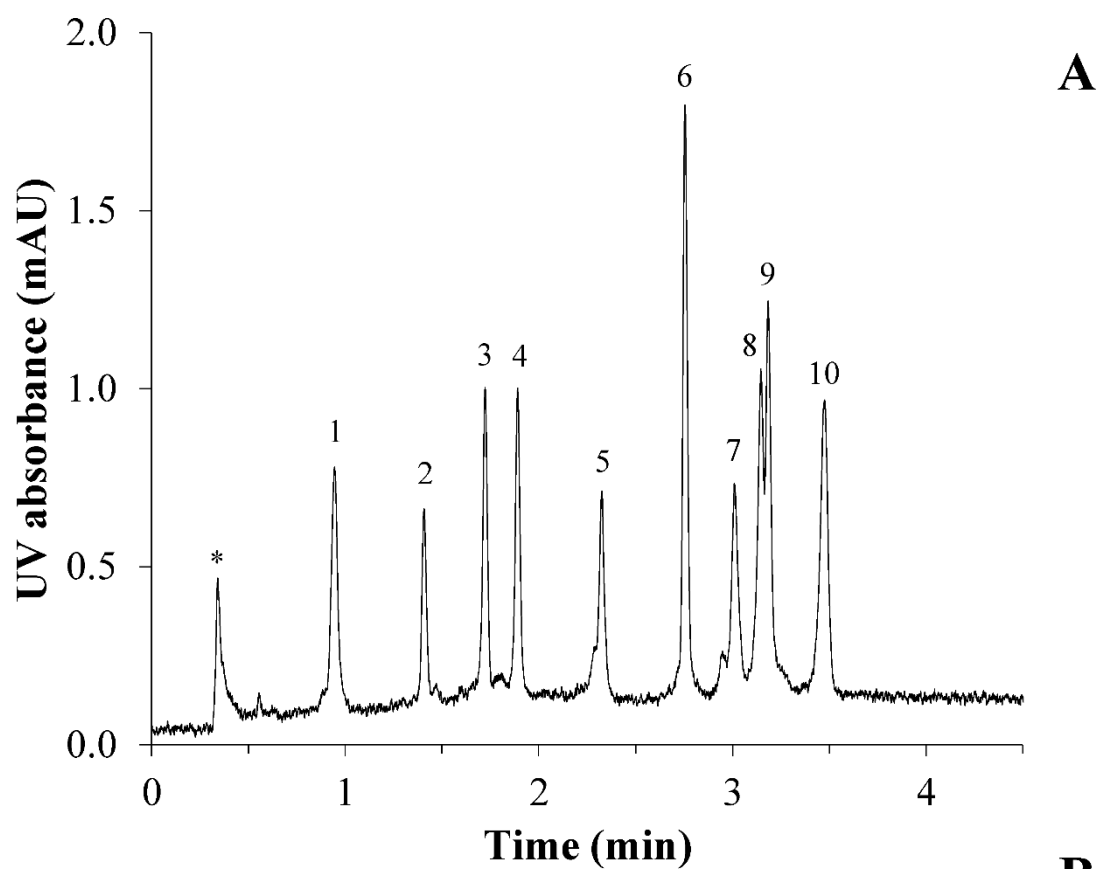
**Figure 2.** SEM images of cross sections of monolithic poly(S-*co*-DVB) structures showing the effect of polymerization temperature (A, B, C) and initiator content (D, B, E). The porogen to monomer ratio was 75:25% (v/v), and the amount of THF was fixed at 21 wt%.



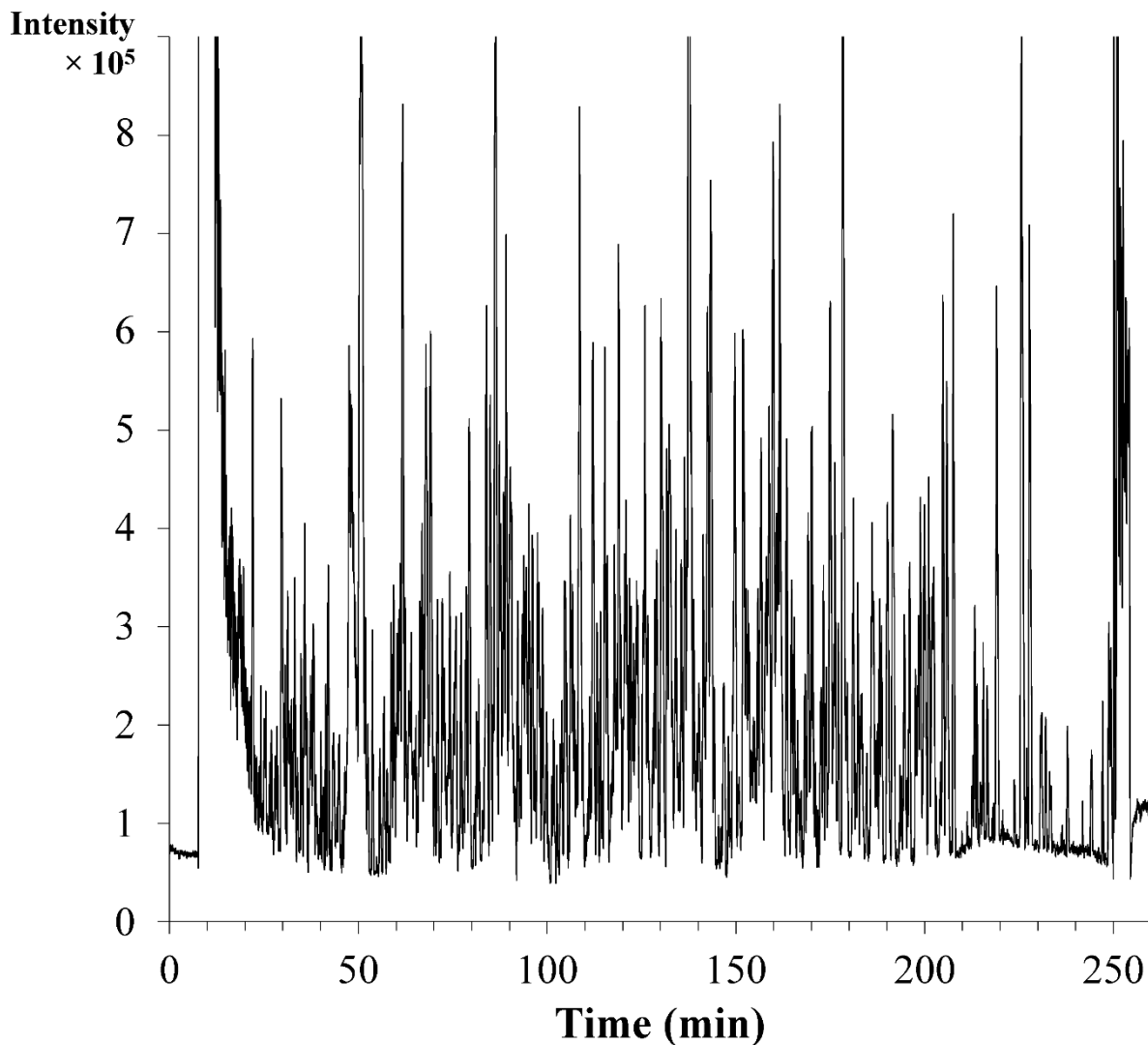
**Figure 3.** Effect of THF content in the porogen on eddy dispersion (A-term, black closed circles) and mobile-phase mass transfer ( $C_m$ -term, black open circles) contributions and resulting average microglobule sizes (red closed circles). Experimental details regarding dispersion characteristics can be found in Fig. S3 and Table S1 in the Supplementary Material.



**Figure 4.** Comparison of the kinetic performance limits in isocratic mode for (A) high-porosity monoliths synthesized with different THF content (18-26 wt%) in the porogen mixture and for (B) the optimized monolithic support structure (21 wt% THF) compared to columns packed with core-shell particles and silica-monolithic materials. Chromatographic properties for the construction of the kinetic plots of packed and silica monolithic parameters were as follows: 1.5  $\mu\text{m}$  core-shell particles:  $A = 1.00 \mu\text{m}$ ,  $B = 3.25 \text{ mm}^2 \cdot \text{s}^{-1}$ ,  $C = 0.43 \text{ ms}$ ,  $K_v = 3.81 \times 10^{-15} \text{ m}^2$  [35]; 2.6  $\mu\text{m}$  core-shell particles:  $A = 2.47 \mu\text{m}$ ,  $B = 3.00 \text{ mm}^2 \cdot \text{s}^{-1}$ ,  $C = 0.51 \text{ ms}$ ,  $K_v = 1.50 \times 10^{-14} \text{ m}^2$  [35]; first-generation silica monoliths:  $A = 6.19 \mu\text{m}$ ,  $B = 4.27 \text{ mm}^2 \cdot \text{s}^{-1}$ ,  $C = 1.38 \text{ ms}$ ,  $K_v = 7.38 \times 10^{-14} \text{ m}^2$  [37]; second-generation silica monoliths:  $A = 2.42 \mu\text{m}$ ,  $B = 4.06 \text{ mm}^2 \cdot \text{s}^{-1}$ ,  $C = 1.11 \text{ ms}$ ,  $K_v = 2.68 \times 10^{-14} \text{ m}^2$  [37]. A maximum operating pressure of 200 bar was applied for the silica monoliths. For all the plots, a molecular diffusion coefficient  $D_m = 1 \times 10^{-9} \text{ m}^2 \cdot \text{s}^{-1}$  and viscosity  $\eta = 0.00056 \text{ Pa} \cdot \text{s}^{-1}$  were applied.



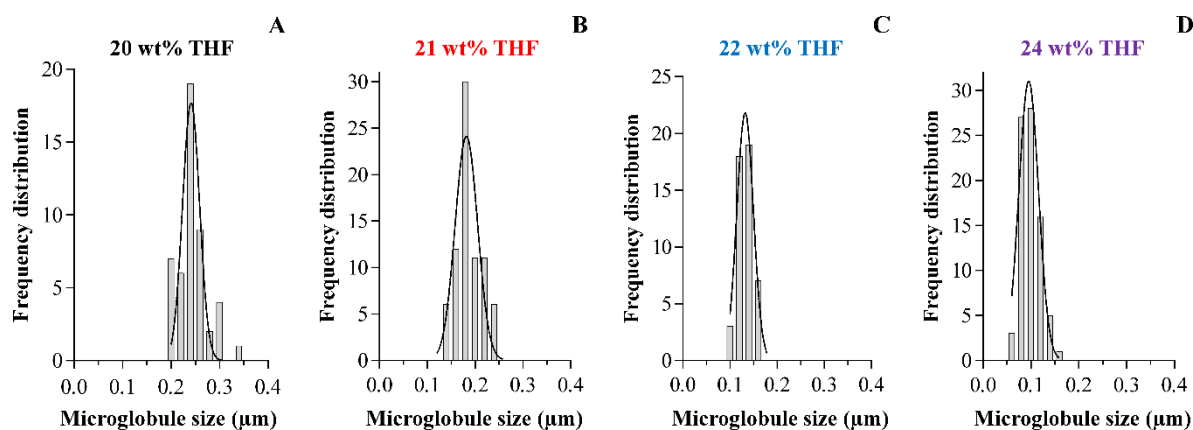
**Figure 5.** (A) Gradient separation of a mixture of 10 intact proteins at a flow rate of 1.5  $\mu\text{L}\cdot\text{min}^{-1}$  and applying a gradient time of 4.68 min from 25-60% B ( $\Delta c = 0.28$ ). (B) In series (5x) gradient separations of a mixture of 6 intact proteins applying a flow rate of 12  $\mu\text{L}\cdot\text{min}^{-1}$  and a ballistic gradient time of 6 s from 25-57% B ( $\Delta c = 0.26$ ), operated at  $\Delta P_{\text{max}} = 400$  bar. Peak identification: (\*) injection solvent, (1) ribonuclease A, (2) insulin, (3) cytochrome *c* equine, (4) cytochrome *c* bovine, (5) trypsin, (6)  $\alpha$ -lactalbumin, (7)  $\alpha$ -chymotrypsin A, (8)  $\alpha$ -chymotrypsinogen A, (9) myoglobin, and (10) carbonic anhydrase. Column length was 70 mm. The injected mixture (4 nL) contained 200 pg of each protein.



**Figure 6.** Base peak chromatogram showing a high-efficiency gradient separation of an *E. coli* digest using a high-porosity monolithic column with a total length of 920 mm, operating at the kinetic performance limit ( $\Delta P_{\max} = 400$  bar). Experimental conditions:  $F = 750$  nL·min<sup>-1</sup>,  $t_g = 240$  min ranging from 1-35% B, and 1  $\mu$ L injection (protein concentration prior to digestion = 0.17  $\mu$ g· $\mu$ L<sup>-1</sup>). 0.1% (v/v) FA was added to the mobile phase as ion-pairing agent.

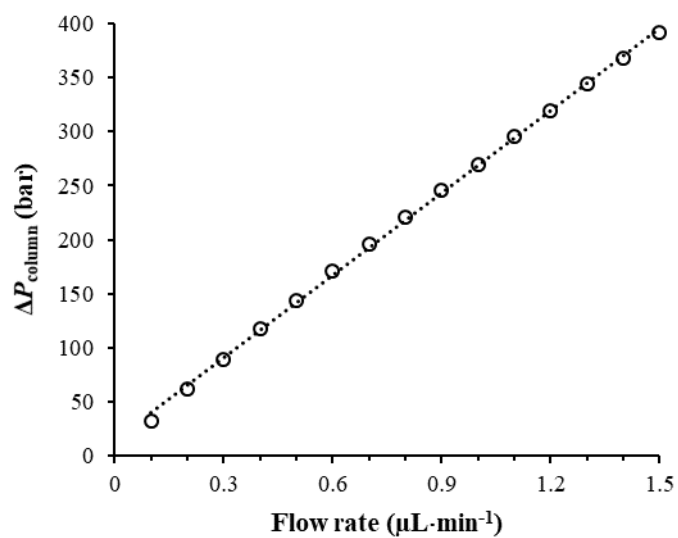
## Supplementary Material

The frequency distribution of the microglobule size of monolithic capillary columns prepared with a porogen to monomer ratio at 75:25% (w/w) while varying the THF porogen content is depicted in Figure S1. SEM images were loaded in ImageJ (NIH, USA) and straight lines ( $n \geq 50$ ) corresponding to the diameter of the microglobules were manually drawn. The measured pixels were calibrated by setting the scale with the correct unit ( $\mu\text{m}$  or nm). The frequency distribution of the size of the microglobules was plotted using Graphpad Prism 6 software program (San Diego, CA, USA). Since the frequency distribution did not pass the normality test, a non-linear Gaussian-type curve was applied with 95% confidence interval using a least-squares fitting method.



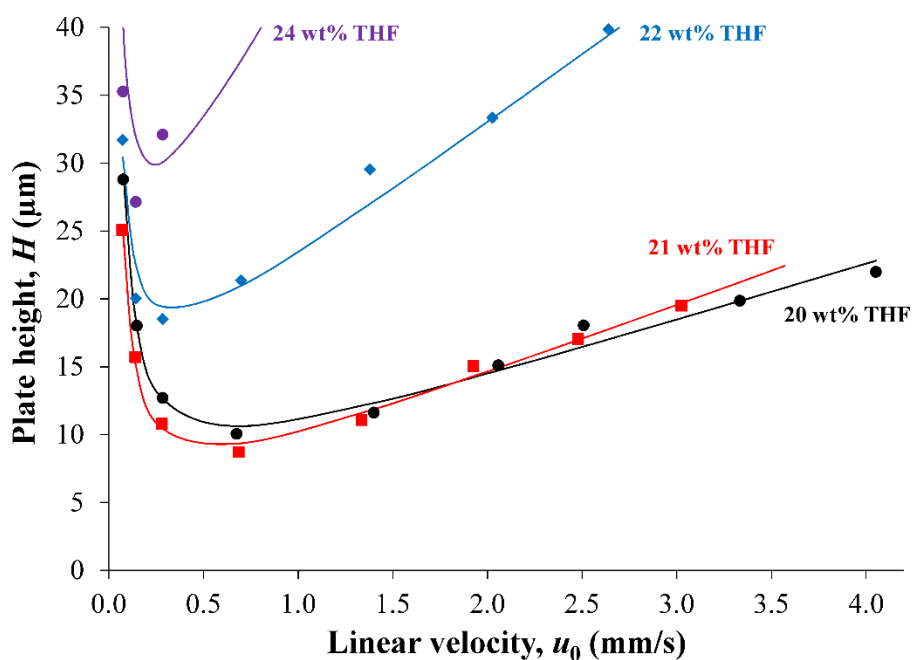
**Figure S1.** Frequency distribution of the microglobule size (in  $\mu\text{m}$ ) estimated based on scanning electron micrographs (SEM), obtained from  $n \geq 50$ , of monolithic poly(S-co-DVB) capillary columns prepared with a porogen to monomer ratio at 75:25% (w/w)% and synthesized with (A) 20 wt%, (B) 21 wt%, (C) 22 wt%, and (D) 24 wt% of THF. The black lines show a fitted Gaussian-type distribution based on the frequency distribution with 95% confidence interval using a least-squares fitting method.

Figure S2 shows the plot of column backpressure of the porous monolithic support structure synthesized with 21 wt% THF in the porogen, as function of the flow rate. The polymer monolithic column showed pressure stability (linear increase) over the range of flow rates applied ( $R^2 = 0.9992$ ).



**Figure S2.** Plot of column backpressure ( $\Delta P_{\text{column}}$ ) as function of flow rate, applying 99% of mobile phase B of 80:20% (v/v) ACN:H<sub>2</sub>O, and using a 100  $\mu\text{m}$  i.d. capillary monolithic column (21 wt% THF in the porogen) with a total length of 920 mm.

The efficiency as function of linear velocity of the monolithic columns was recorded by injecting a  $t_0$ -marker (uracil), applying a mobile phase of 80:20% (v/v) ACN:H<sub>2</sub>O, see the van Deemter curves depicted in Fig. S3. The extra column dispersion was minimized by mounting the column directly on the stator of a 4 nL valve and using 20  $\mu\text{m}$  i.d.  $\times$  100 mm connection tubing towards a 3 nL UV flow cell. The monolithic column synthesized with 21 wt% THF yielded a minimum plate height of 8.7  $\mu\text{m}$  at optimum mobile-phase velocity, being able to generate  $\sim 115,000$  plates/meter. Chromatographic dispersion could not be further improved by changing the porogen ratio. When pursuing the synthesis of sub-200 nm globules and macropores, both  $A$ - and  $C_m$ -term contributions increase, which it is related to structure inhomogeneity.



**Figure S3.** van Deemter curves recorded for uracil while applying 80:20% (v/v) ACN:H<sub>2</sub>O on polymer monolithic columns synthesized with 20 wt% (black), 21 wt% (red), 22 wt% (blue), and 24 wt% of THF (purple) in the polymerization precursor mixture. A non-linear fit of the van Deemter curve was applied to the experimental data, with least-squares fitting by minimizing the residuals, see Table S1.

Table S1 summarizes the different chromatographic properties of the synthesized monolithic columns.

**Table S1.** Chromatographic properties of the different monolithic poly(S-*co*-DVB) capillary columns

S (wt%)	DVB (wt%)	1-Dec (wt%)	THF (wt%)	AIBN (wt% <sup>a</sup> )	$T_p$ <sup>b</sup> (° C)	$d_{\text{microglobule}}$ ( $\mu\text{m}$ )	$K_v$ ( $\text{m}^2$ )	A ( $\mu\text{m}$ )	C (ms)	$H_{\text{min}}$ ( $\mu\text{m}$ )	$E_{\text{min}}$
12.5	12.5	57	18	3	70	1.06	$2.57 \times 10^{-12}$	17.1	26.1	27.6	297
12.5	12.5	55	20	3	70	0.25	$7.84 \times 10^{-14}$	5.1	4.3	10.1	1290
12.5	12.5	54	21	3	70	0.19	$7.78 \times 10^{-14}$	3.6	5.2	8.7	976
12.5	12.5	53	22	3	70	0.13	$3.01 \times 10^{-14}$	12.0	10.2	18.5	11392
12.5	12.5	51	24	3	70	0.10	$9.73 \times 10^{-15}$	15.7	29.3	27.1	75676
12.5	12.5	49	26	3	70	0.07	$4.77 \times 10^{-15}$	46.4	50.2	50.3	531109
12.5	12.5	54	21	2	70	0.14	$10.14 \times 10^{-14}$	7.0	4.3	10.8	1141
12.5	12.5	54	21	4	70	0.10	$5.01 \times 10^{-14}$	3.7	3.9	8.5	1457
12.5	12.5	54	21	3	65	0.46	$6.18 \times 10^{-13}$	10.9	12.6	15.4	382
12.5	12.5	54	21	3	75	0.07	$1.68 \times 10^{-14}$	4.8	11.6	14.0	11656

<sup>a</sup> With respect to the monomer content

<sup>b</sup> Polymerization temperature

The construction of kinetic plots incorporates the transformation of experimental measurements obtained on a single column length and varying column pressure towards the kinetic performance limits when applying longer columns at a fixed (maximum) column pressure. To demonstrate the validity of this approach in gradient mode, the kinetic performance limits were extrapolated based on data obtained on a 70 mm long column yielding a minimum separation impedance in isocratic mode of 976, and by measuring gradient performance data conducting coupled-column experiments, *i.e.*, coupling a maximum of four 230 mm long columns and scaling  $t_G/t_0$  such that the gradient volume was fixed at all experiments ( $t_G/t_0 = 5$ ) applying a maximum operating pressure of 400 bar. Table 1 in the main manuscript displays the direct quantitative comparison of predicted and experimental peak capacities, determined via the average 4 sigma peak width ( $W$ ) and applying  $n_c = (t_G/W_b) + 1$ .